JOURNAL OF MATERIALS SCIENCE **38** (2003) 767–777

# Microstructurally controlled mullite ceramics produced from monophasic and diphasic sol-derived pastes using extrusion

C. KAYA*, E. G. BUTLER
*Interdisciplinary Research Centre (IRC) in Materials Processing, The University of Birmingham, Edgbaston, Birmingham B15 2TT, UK*
*E-mail: c.kaya@bham.ac.uk*

M. H. LEWIS
*Department of Physics, Centre for Advanced Materials, University of Warwick, Coventry CV4 7AL, UK*

Mullite ceramics with controlled microstructure in terms of grain size/shape, pore and glassy phase content were produced from sol-derived pastes using extrusion. Particular attention has been given to the development of a continuous process which is suitable for the preparation of high-solids-loading mullite pastes from two different starting mullite precursors, namely, diphasic and molecular mixed mullite sols. A combined processing technique comprising vacuum filtering and pressure filtration was introduced in order to obtain extrudable mullite pastes from low solids-loading colloidal sols. It is shown that glassy phase free stoichiometric 3:2 mullite ($3Al_2O_3 \cdot 2SiO_2$) with fine (0.94 $\mu$m) equiaxed grain microstructure is achievable from monophasic precursors after pressureless sintering at 1400°C for 3 h using the developed technique which can control both the sol-derived paste microstructure and process parameters. It is also found that the room and high temperature (1300°C) flexural strength and toughness of extruded mullites are mainly controlled by the grain size, the presence and location of glassy phase, nano-inclusions and pores at the grain boundaries. Pressureless sintered mullite derived from the monophasic sol-derived pastes provides flexural strength values of 345 and 277 M Pa for room temperature and 1300°C, respectively. 

## 1. Introduction

Stoichiometric and glassy phase free mullite ($3Al_2O_3 \cdot 2SiO_2$) exhibits high refractoriness, low creep rate, low thermal expansion coefficient ($4–5 \times 10^{-6}$ $C^{-1}$) and dielectric constant ($\varepsilon = 6–6.7$), low thermal conductivity, good chemical and thermal stability as well as good thermal shock resistance and high temperature structural properties [1]. Mullite ceramics produced from chemically synthesised mullite powders/sols posses better mechanical properties due to improved chemical homogeneity and finer particle size together with better control of particle morphology of the starting precursor resulting in enhanced sinterability at lower temperatures [2].

Two main starting precursors are widely used in the fabrication of mullite ceramics, i.e., colloidal mullite or so-called 'diphasic gels' which usually contains a mixture of boehmite and amorphous silica [3–7] and molecular mullite or so-called 'single-phase gels' that refer to molecular mixture of Al-Si-O [8–10]. When the colloidal approach is used in diphasic gels, orthorombic mullite can be formed in the range of 1150–1350°C via direct reaction of alumina-rich and silica-rich components of the gel. Colloidal processing of diphasic mullite reduces the sintering temperature as a result of increased chemical homogenity, the absence of particle aggregates, and the development of a uniform green microstructure. The reaction rate can be increased by using nano-size alumina in the form of boehmite and amorphous silica phases, leading to the formation of shorter mass transport distances. On the other hand, single-phase gels are normally derived from aluminum and silicon salts and alkoxides, but the experimental conditions have to be engineered carefully to avoid component segregation due to differences in hydrolysis rate of the constituents. Single-phase gels exhibit molecular scale mixing of Al and Si ions, as a result of the formation of Al–O–Si bonding that occurs in the gel, consequently the mullite formation temperature can be further reduced [8–10].

One of the main objectives of the present work is to develop a glassy-phase-free mullite with controlled microstructure in terms of the grain size and porosity content using both diphasic and monophasic mullite

*Author to whom all correspondence should be addressed.

starting precursors. An extrusion technique is used as a powerful tool for producing mullite extrudates with high green and sintered densities from the sol-derived pastes. A new combined technique comprising vacuum filtering and pressure filtration was also introduced and effectively used to form extrudable mullite pastes from nano-size sols.

## 2. Experimental work

### 2.1. Mullite precursor materials

The chemical composition and physical properties of the starting materials used are shown in Table I. It is

TABLE I Chemical composition and physical properties of mullite precursors used

| | Siral 28M[a] | Bacosol 75A[b] |
|---|---|---|
| $Al_2O_3$ (wt%) | 71.6 | 72.7 |
| $SiO_2$ (wt%) | 28.4 | 26.3 |
| $Na_2O$ (%) | 0.01 | 0.55 |
| $Fe_2O_3$(%) | 0.01 | <0.05 |
| Surface area (BET) ($m^2/g$) | 338 | 200 |

[a]Condea Chemie GmbH, Germany, Siral 28M is a molecular mixture of Al—Si—O ions (monophasic gel) based on the following formulation; $(Al_2O_3)x \times (SiO_2)y \times (H_2O)z$.
[b]Alcan Chemicals Ltd., UK, Bacosol 75A is obtained by mixing boehmite and silica sols (diphasic gel).

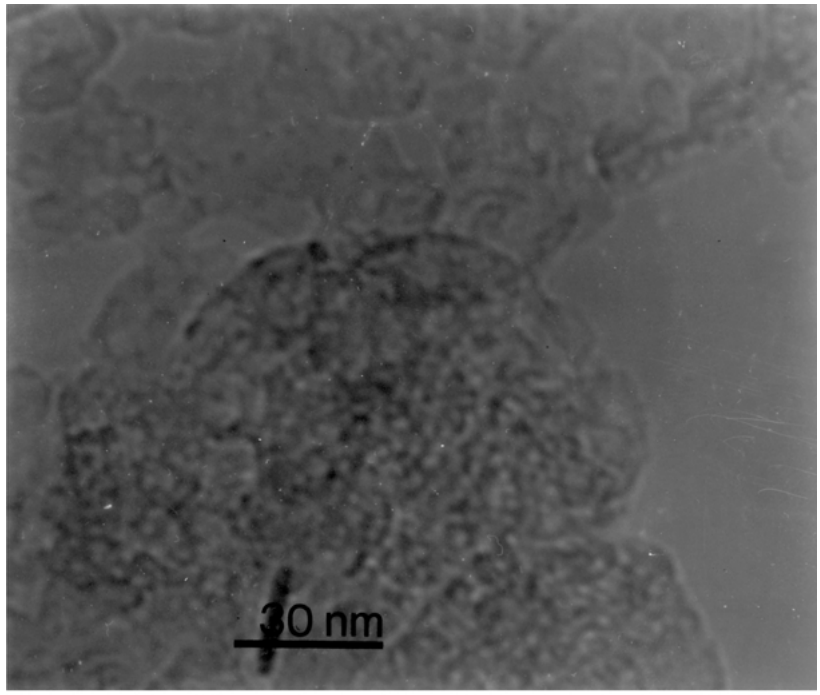


(a)

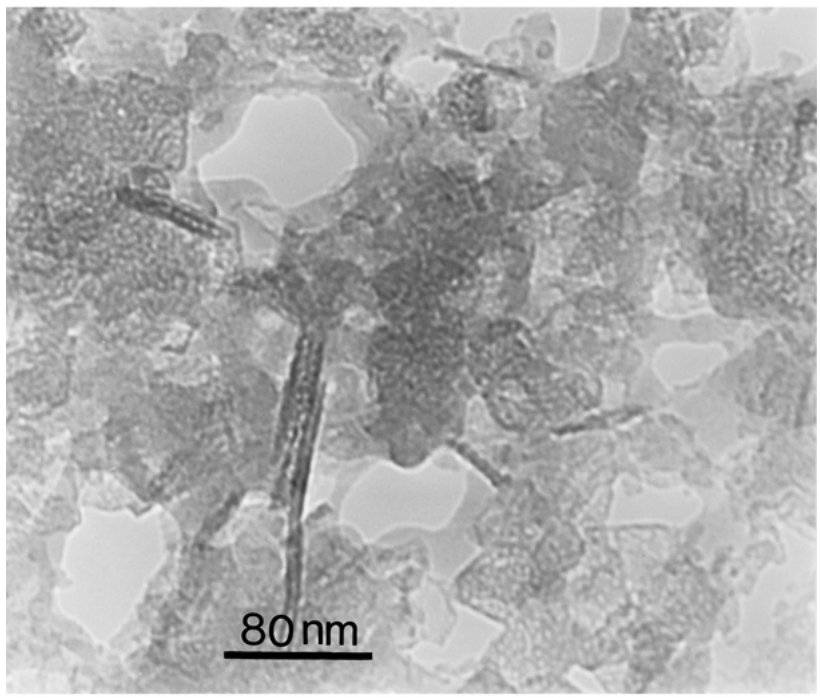


(b)

*Figure 1* TEM micrographs of (a) monophasic (28M) and (b) diphasic (75A) mullite gel structures after heating at 900°C for 2 h.

very well established today that even small amount of contamination or glassy phase within the mullite matrix results in a dramatic decrease in mechanical performance at high temperature, thus very pure starting materials were chosen as shown in the Table I. Bacosol 75A (diphasic gel, will be named 75A hereafter) is obtained by mixing boehmite (40 nm) and silica (20 nm) sols in proportion to obtain stoichiometric mullite composition. Siral 28M is a molecular mixture of Al–Si–O ions (monophasic gel, will be named 28M hereafter) based on the following formulation:

$$(Al_2O_3)_x \times (SiO_2)_y \times (H_2O)_z$$

## 2.2. Sol-derived paste preparation and extrusion

The received 28M mullite powders were first dispersed in distilled water and 5 wt% nano-size zirconia powders with an average particle size of 30 nm (VP zirconia, Degussa Ltd, Germany) in the form of TZP with addition of 3 mol% $Y_2O_3$ (average particle size is 15 nm) were added to the sol (in order to obtain TZP particles, $Y_2O_3$ and zirconia powders were first dispersed in distilled water separately and then added to the suspension containing 28M powders). A small amount of additions was also made and the details are given in Table II. Celacol was first dissolved in hot water (at 80°C in 80 ml water) and then added to the suspension. Glycerol

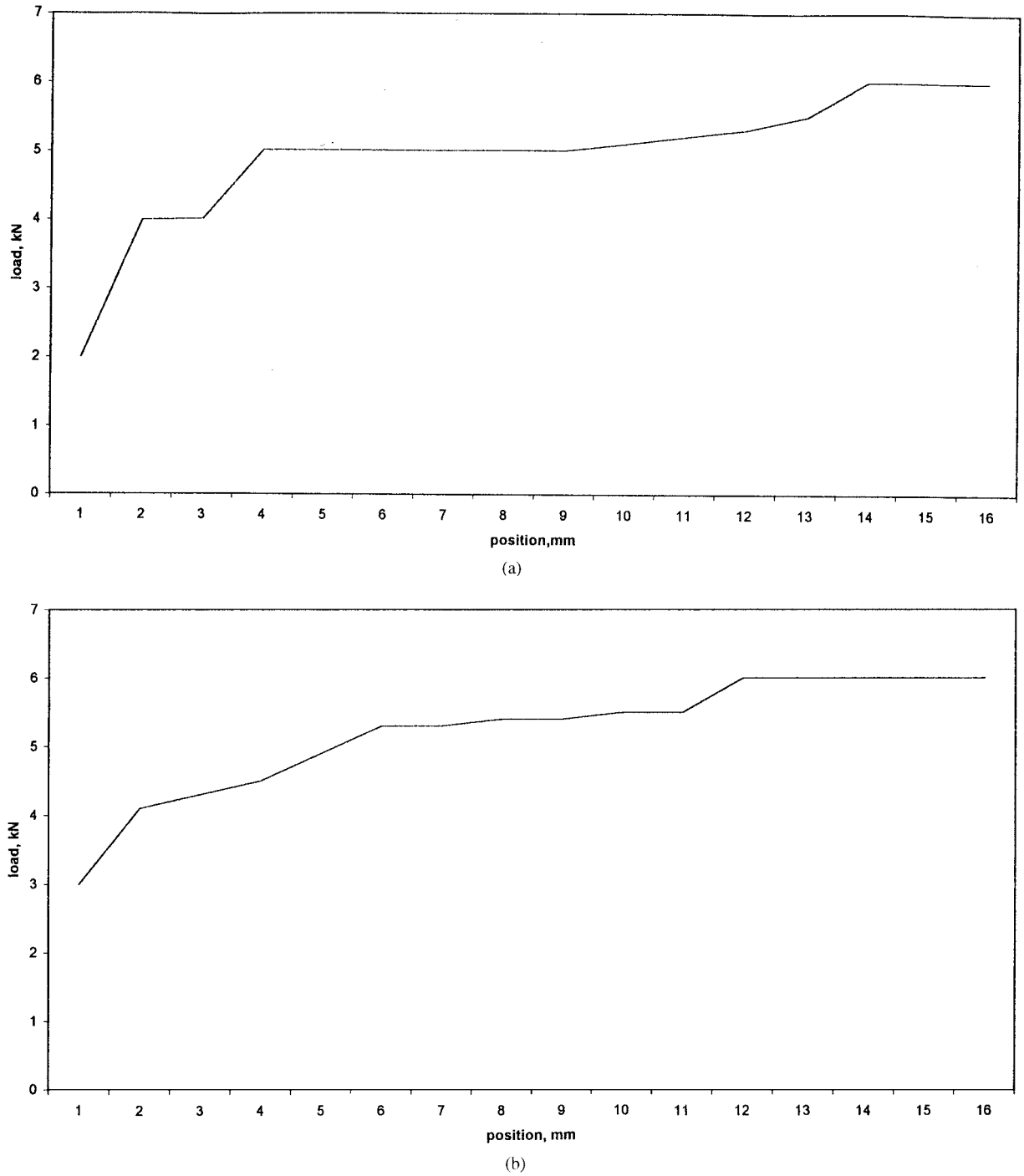


*Figure 2* Sol paste rheology for (a) monophasic (28M) and (b) diphasis (75A) mullite pastes during extrusion.

TABLE II The final composition of 28M (monophasic gel) and 75A mullite (diphasic gel) suspension

| |
|---|
| * Distilled water + 28M powders or 75A sol |
| * 5 wt% zirconia powder |
| * 3 mol % $Y_2O_3$ powder |
| * Celacol (first dissolved in water at 80°C), 1 wt% |
| * Glycerol, 1 wt% of the total powder |
| * Cyclohexanone ($C_6H_{10}O$), 1 wt% |

and cyclohexanone were added to obtain a smooth extruded surface, acting as lubricants. Kinetically stable and well-dispersed suspensions having 20 wt% solids-loading were obtained at a pH value of 3.5. Similar additions were made to 75A mullite sol in order to obtain extrudible pastes (see Table II).

The final composition was first ball-mixed using high purity zirconia balls for 1 day and then vacuum filtered to obtain a gel structure. After the ball-milling, no particles coarser than 300 nm were detected by the particle size anlysis indicating that both mullite sols are free of heteroflocculated chains in the sol state. The obtained gel was then pressure filtrated leading to the formation of high solids-loading extrudible mullite pastes. Extrusion experiments were carried out using a laboratory scale extrusion die at an extrusion rate of 1 mm/min. Extruded rods were first kept in humidity controlled chamber for 1 day, then in air for 1 day and then sintered at 1400°C on a grooved sintering plates for 3 hours.

## 2.3. Other characterisation techniques

Powders and sintered samples were analysed using X-ray diffraction (Cu $K_\alpha$ radiation and nickel filter to remove the Cu $K_\beta$ peak, Philips X'Pert, Germany), operated at 40 keV and 30 mA. The diffractometer scanned from 5° to 80° with a scan step of 0.02° $2\theta$ and a count time of 2 seconds per step. Phase identification was carried out using a computer controlled X-ray diffractometer and obtained peaks were compared with the $d$-spacing for standard phase compositions listed in the JCPDS-ICDD archive. Powder samples were subjected to differential thermal analysis (DTA) and thermal gravimetric analysis (TGA) under static air atmosphere using a Stanton Redcroft STA781 simultaneous DTA/TGA apparatus in order to determine the phase transformation temperatures and related mass

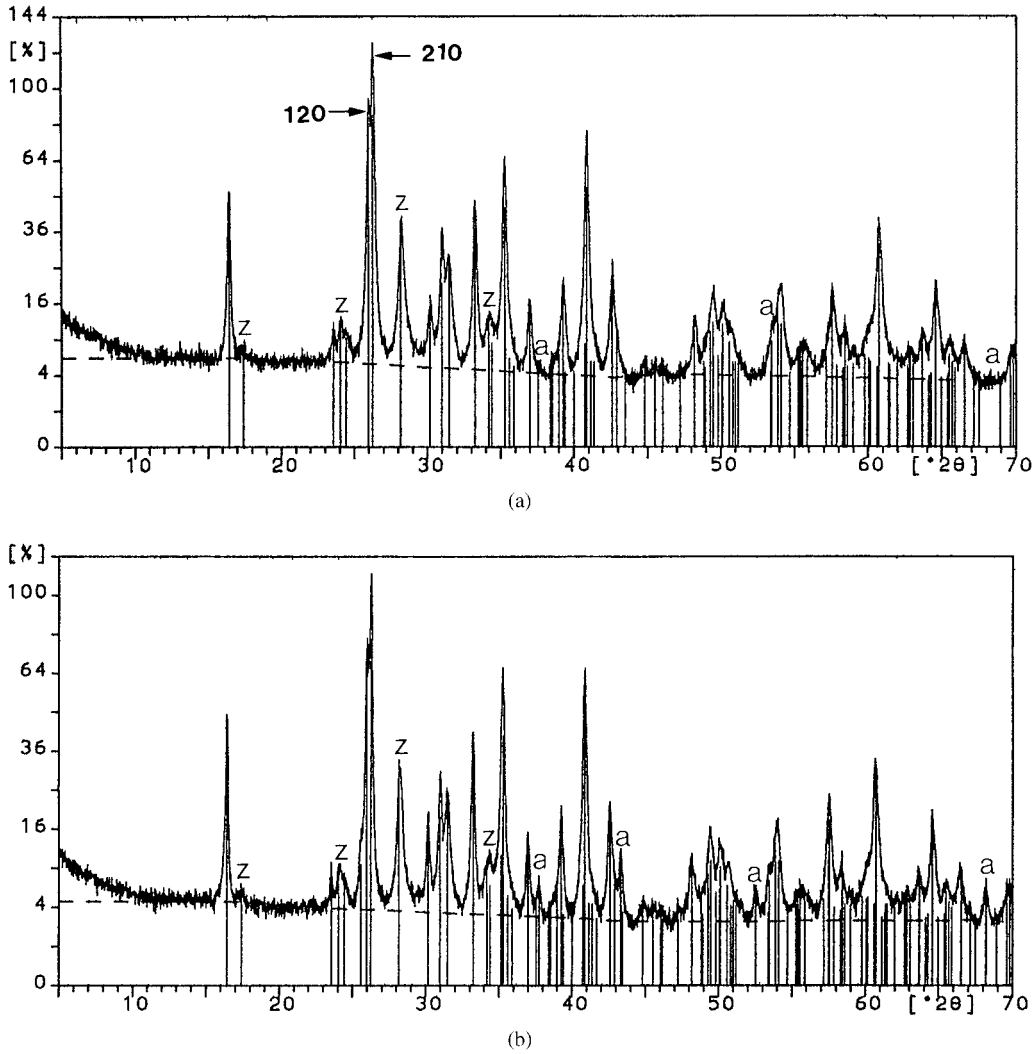


*Figure 3* X-ray (Cu $K_\alpha$) diffraction patterns for sintered samples produced from (a) 28M and (b) 75A sol-derived mullites showing the presence of stoichiometric 3:2 mullite with some minor peaks of alumina and zirconia after sintering at 1400°C for 3 h (a: $\alpha$-alumina, z: monoclinic or tetragonal zirconia, the other peaks represent 3:2 mullite).

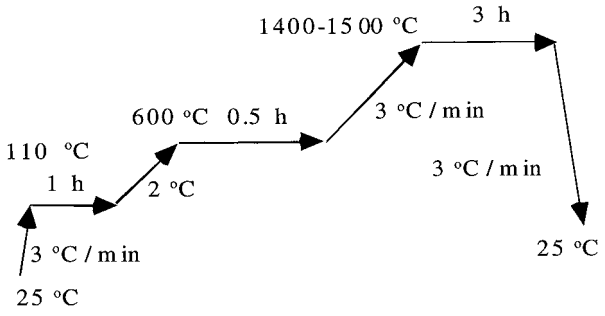


*Figure 4* Sintering cycle for sol-derived mullite extrudates.

loss. High purity $\alpha$-alumina was used as a reference material. Phase transformation temperatures and mass loss due to reaction were measured by a thermocouple and an electronic hang-down balance, respectively. These data were collected and analysed using a computer linked to the equipment. All experiments were carried out using a fixed sample mass (10 to 15 mg $\pm$ 0.01 mg) and heating rate (10°C/min). Microstructural examinations on sintered samples were carried out using a Field Emission Gun SEM (FEG SEM FX-4000, Jeol Ltd. Japan) and transmission electron microscopy (Philips CM 20, Germany).

Sintered densities were measured using the Archimedes technique. Room and high temperatures 4-point bend strength of the sintered samples were measured with a computer controlled Instron testing machine with a 20 mm inner and 40 mm outer span and a cross-head speed of 0.5 mm $\cdot$ min$^{-1}$. For high temperature tests, after reaching the test temperature, the sample was kept at that temperature for 30 min. and then the test was conducted. 6 samples were tested

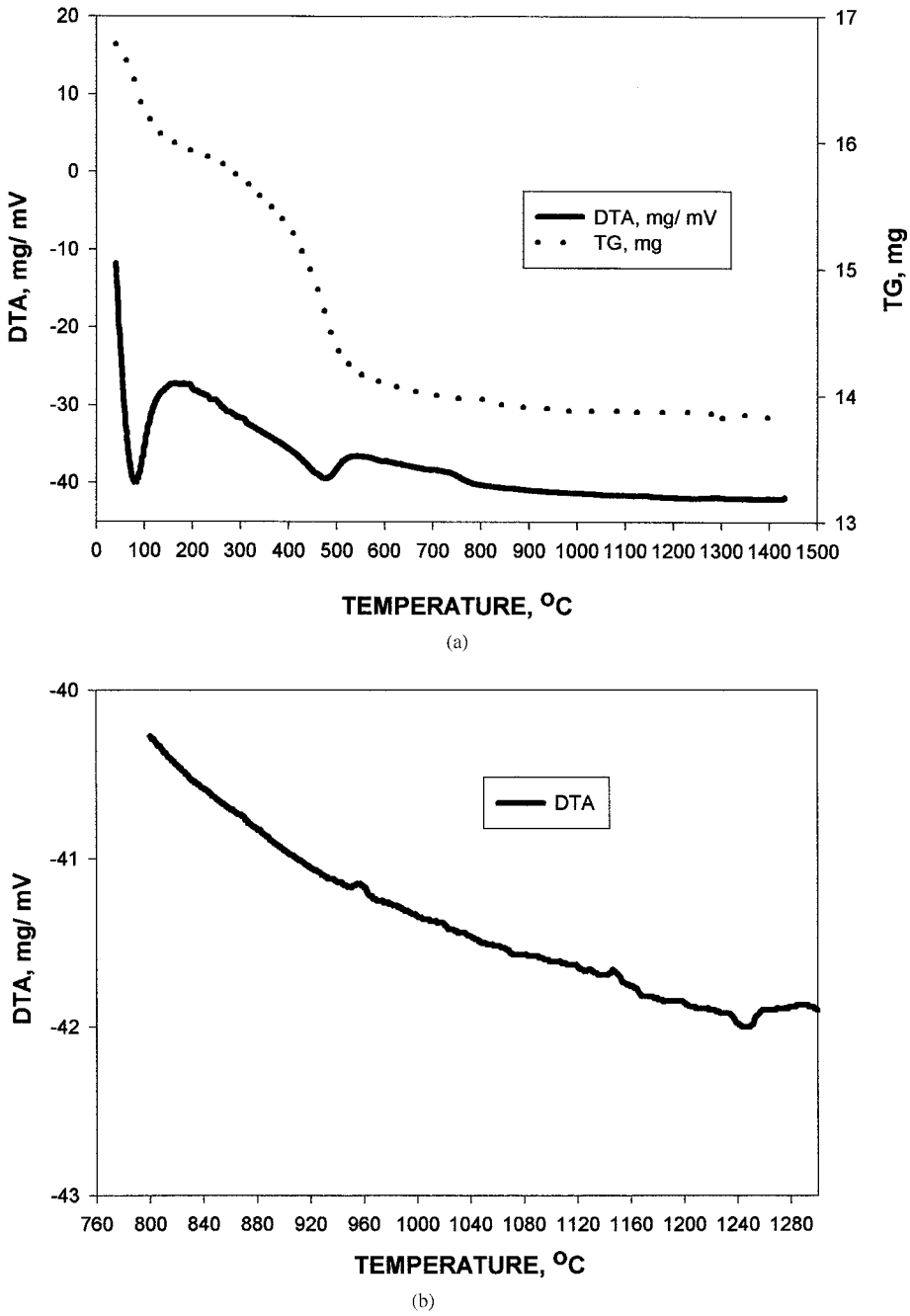


*Figure 5* (a) DTA and TGA traces for the 28M monophasic mullite and (b) DTA trace for the 28M monophasic mullite sol showing the reaction temperatures in the temperature region of 800–1300°C.

for each temperature and the average strength was reported. The following equation was used to measure the flexural strength of the rods:

$$\sigma = \frac{8F(S_2 - S_1)}{\pi d^3} \quad (1)$$

where $F$ is the failure load, $S_2$ and $S_1$ are the outer and inner span lengths, respectively and $d$ is the diameter of the extrudate rod. Fracture toughness was measured using Vicker's indentation technique [11]. Linear intercept technique was used to measure the average mullite grain size on polished and thermally etched surfaces [12].

## 3. Results and discussion

Bright-Field TEM images of molecular mixed (28M) and diphasic (75A) mullite gel microstructures after heating at 900°C for 2 h, are shown in Fig. 1a and b, respectively. The amorphous and interconnected two-phase nature of 28M mullite after heating is clearly visible from the micrograph shown in Fig. 1a. Fig. 1a also shows that the molecular mixed mullite gel remains quite porous after heat treatment due to decomposition and dehydration of organic components. On the other hand, the 75A mullite gel which is a mixture of boehmite and silica particles remains amorphous after heating and individual nano-size boehmite and silica particles can easily be identified from the

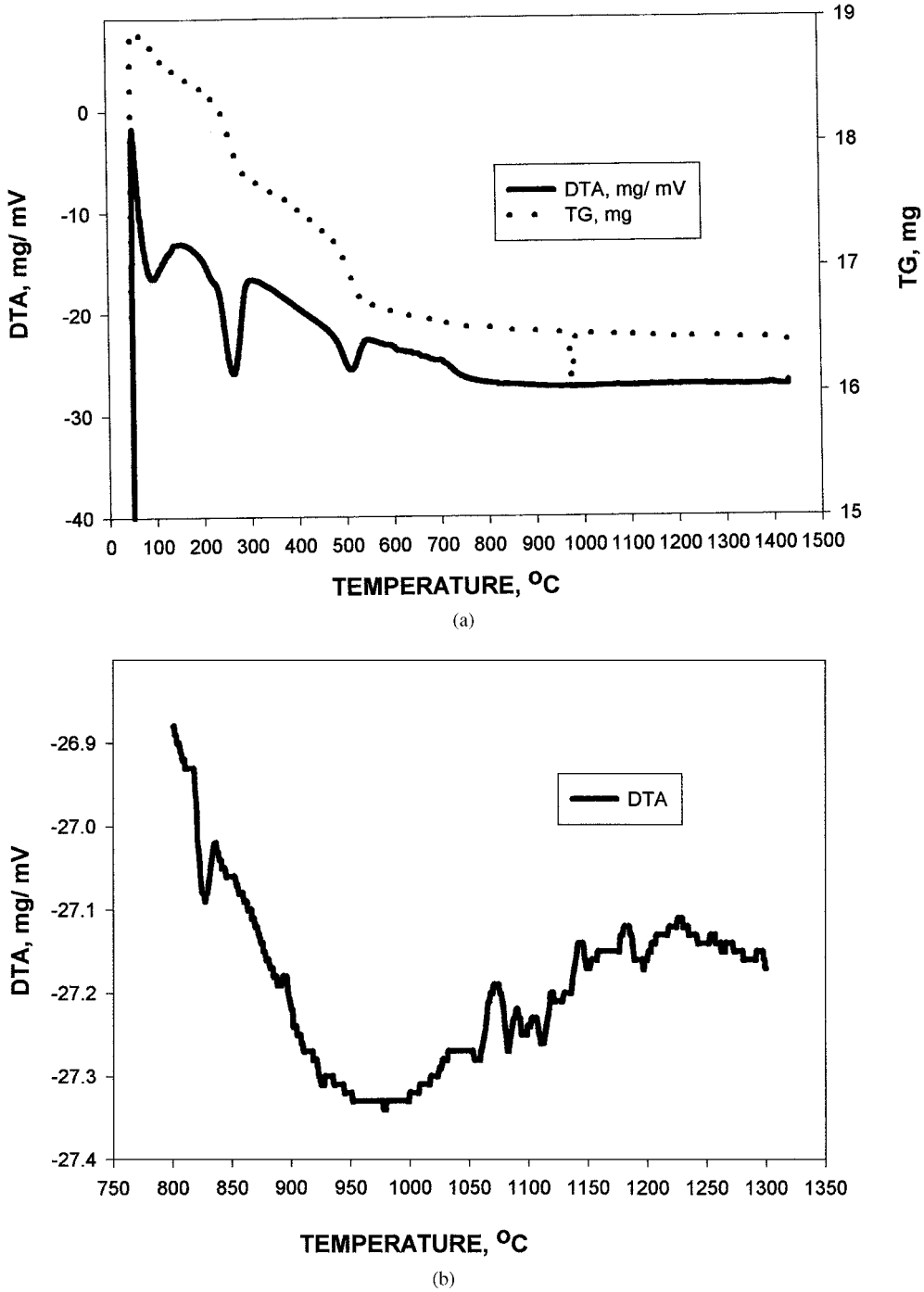


*Figure 6* (a) DTA and TGA traces for the 75A diphasic mullite and (b) DTA trace for the 75A diphasic mullite showing the reaction temperatures in the temperature region of 800–1300°C.

image shown in Fig. 1b. However, the boehmite particles shown in Fig. 1b exhibit transitional alumina structure after heat treatment resulting from the transformation of $\gamma$-AlOOH to $\gamma$- and $\delta$-$Al_2O_3$ which causes interconnected pore formation. Overall, both micrographs shown in Fig. 1 indicate the absence of any aggregate formation or preferential separation of boehmite and silica (Fig. 1b).

The load-displacement curves characterising the sol-derived paste rheology for 28M and 75A mullites are given in Fig. 2a and b, respectively. Pastes obtained from the sol containing 28M and 75A compositions showed no "shear thickening" behaviour during extrusion as shown in Fig. 2. It shows that the obtained pastes are homogeneously mixed during the sol preparation steps and there is no excessive liquid migration from the paste which could result in a drop in applied pressure on the barrel during extrusion.

X-ray diffraction patterns for the 28M and 75A extrudates sintered at 1400°C for 3 hours are shown in Fig. 3a and b, respectively (detail sintering cycle is given in Fig. 4). Both materials produced stoichiometric 3:2 mullite peaks, together with additional peaks corresponding to zirconia and small amount of $\alpha$-alumina.

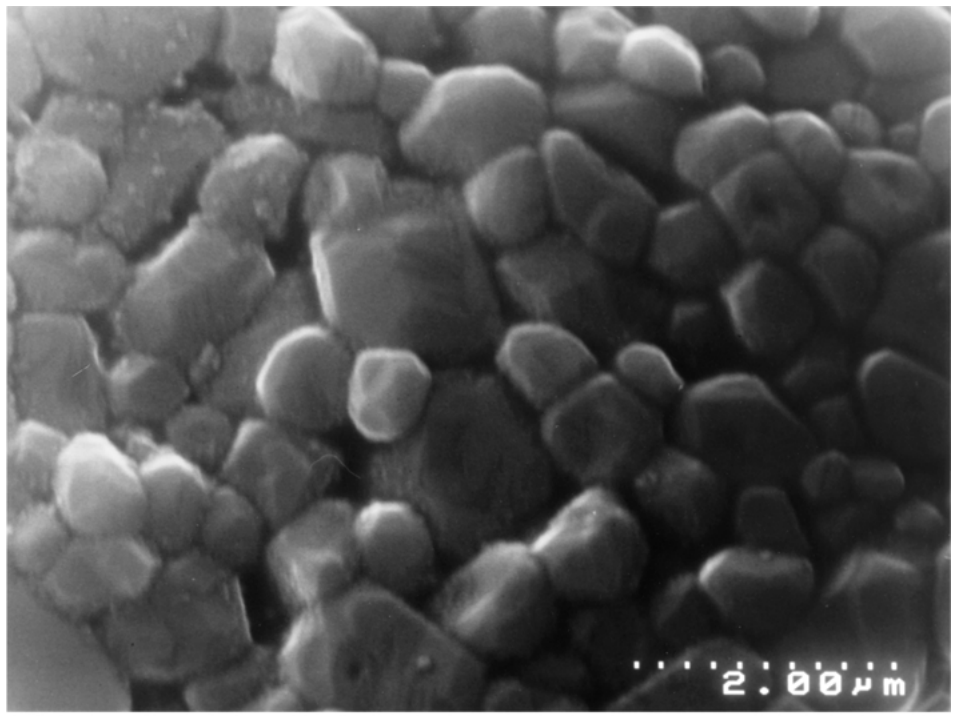


(a)

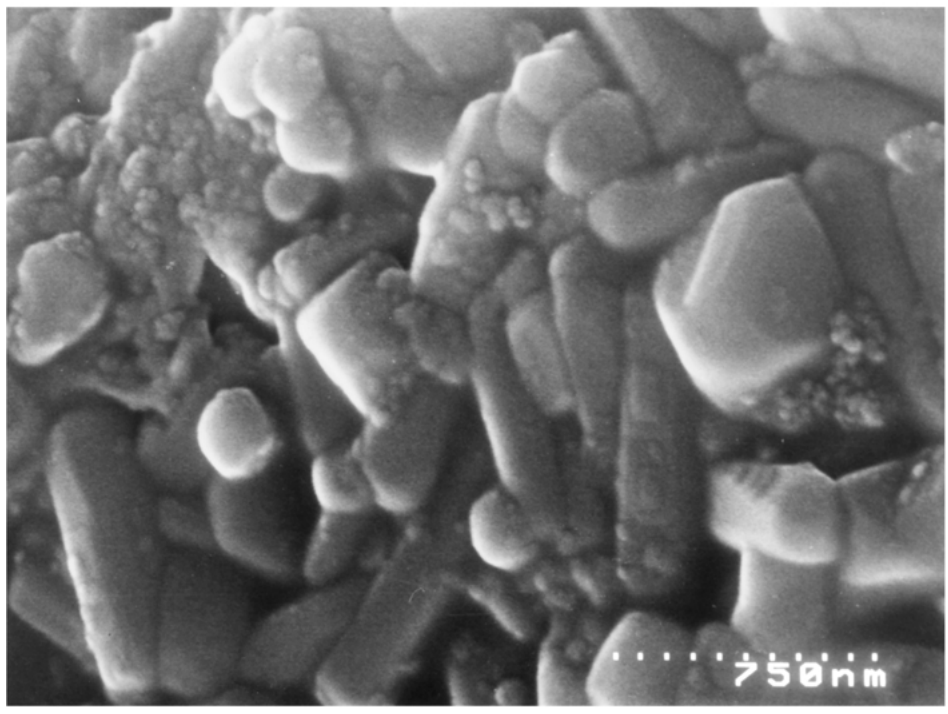


(b)

*Figure 7* SEM micrographs of (a) 28M and (b) 75A mullite extrudates after sintering at 1400°C for 3 h.

As shown in Fig. 4, 1400°C was found to be high enough to produce stoichiometric mullite composition without formation of residual glassy phase within the detection limit of XRD technique.

The DTA and TG traces (heating rate: 10°C/min) for the 28M and 75A powder samples are shown in Figs 5 and 6, respectively. 28M material showed a total weight loss (%) of 17.69 (starting weight: 16.78 mg and finishing weight: 13.81 mg). As can be seen from the graph 5a, the first reaction (and weight loss) occurs at about 120°C and corresponds to the removal of the free water within the powder. Second major weight loss was recorded at about 450–500°C indicating the removal of the crystalline water and OH groups. 28M exhibited minor exothermic peaks at 950°C and 1150°C as well as a broader endothermic peak at 1250°C, as shown in detail in Fig. 5b. The former exotherm corresponds to the formation of an Al-Si spinel or tetragonal mullite ($2Al_2O_3 \cdot SiO_2$) which transforms to orthorhombic mullite at a starting temperature as low as 1150°C [8]. The endothermic peak observed at 1250°C is probably due to the densification of orthorombic mullite as shown in Fig. 5b.

The DTA and TG traces of 75A material are shown in Fig. 6. The total weight loss for 75A was found to be low, about 12.76 (%) of the total mass (starting weight: 18.8 mg and finishing weight: 16.39 mg). The major weight loss and reaction temperatures were determined at 100, 250 and 500°C, corresponding to the removal of the free water (100°C) and crystalline water and OH groups (450–500°C). The presence of an exothermic peak at about 830°C indicates the starting temperatures of Al–Si spinel formation. In diphasic gels, the DTA usually indicates formation of mullite as an exotherm at about 1220–1250°C. As shown in Fig. 6b, there are two major exothermic peaks at 1075 and 1225°C and two minor peaks at 1140 and 1170°C. The former (1075°C) indicates the formation of transitional alumina phase

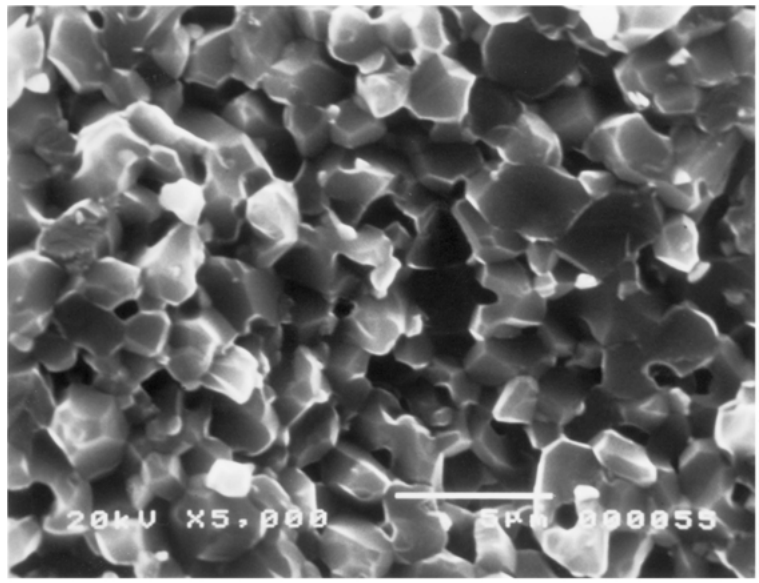


(a)

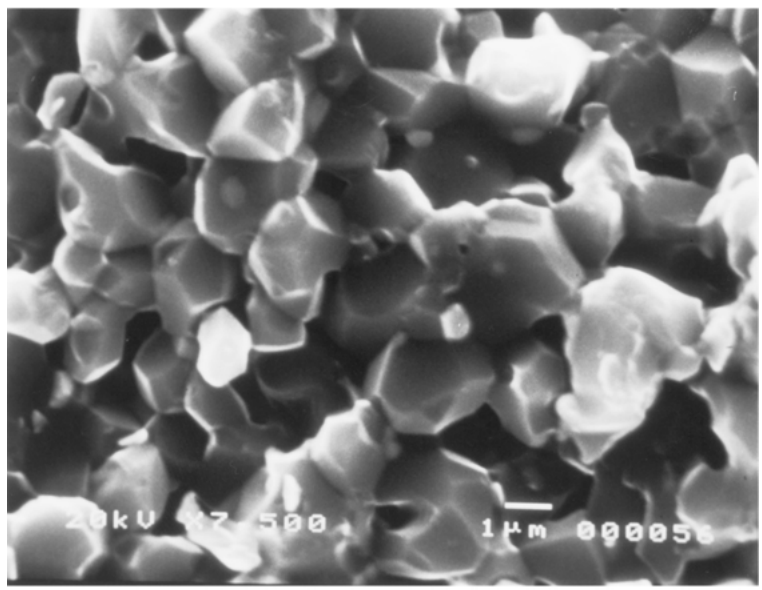


(b)

*Figure 8* SEM micrographs of room temperature fracture surfaces of (a) 28M and (b) 75A mullites showing mainly intergranular fracture mode.

along with silica and the second broad one (1225°C) one represents the formation of mullite phase and subsequent densification. Both minor peaks are due to the formation or transformation of transitional aluminas.

As summarised in Figs 5 and 6, 28M contains molecular mixed precursors, therefore this route is expected to result in the crystallization of the metastable Al–Si spinel directly from the amorphous state. Firstly, a small amount of tetragonal mullite ($2Al_2O_3 \cdot SiO_2$) forms at about 930°C, then these spinel and tetragonal mullite phases transform to stable orthorombic 3:2 mullite at about 1100°C. This transformation process is very slow due to a slow diffusion process and the results found in this work are in good agreement with the previous findings [8–10]. In diphasic gel, i.e., 75A, as shown in Fig. 6, mullite crystallization is preceded by the formation of transient alumina phases ($\gamma$-$Al_2O_3$, silicon-aluminum spinel phase) and occurs via an exothermic reaction at 1225°C.

Fig. 7a and b show SEM images of sintered 28M and 75A mullite specimens, respectively after sintering at 1400°C for 3 hours indicating the dense mullite matrix microstructure. Mullite matrix obtained from 28M contains equiaxed grains with no elongated mullite grains as shown in Fig. 7a, in contrary the sintered matrix of 75A results in some elongated mullite grains as shown in Fig. 7b. The average mullite grain size of 28M and 75A are calculated to be 0.94 $\mu$m and 1.4 $\mu$m, respectively. Fig. 7 also shows that extrusion direction does not affect the grain morphology or alignment in 28M matrix (Fig. 7a) whereas some of the elongated mullite grains are aligned parallel to the extrusion direction as shown in Fig. 7b. The sintered densities (% theoretical density) of 28M and 75A were determined as 96.6 and 96.1, respectively whilst % sintering shrinkage values of 42 and 22 were recorded for 28M and 75A, respectively.

The SEM images of room temperature fracture surfaces of 28M and 75A are shown in Fig. 8a and b respectively, indicating that the dominant fracture mode is intergranular fracture for both mullites. In order to relate the thermomechanical behaviour to the microstructural features of the two type of mullites, detailed TEM and field emission gun SEM observations were carried out on the samples subjected to flexural test at 1300°C. The TEM micrographs of 28M and 75A mullites are shown in Fig. 9a and b, respectively. No glassy phase was observed at the triple grain junction or along the mullite grain boundaries of 28M as shown in Fig. 9a whereas the presence of a glassy phase at the triple grain junction of mullite grains within 75A is evident from the image shown in Fig. 9b. As shown in Table III, 28M mullite loses almost 20% of its room temperature strength at 1300°C (from 345 MPa to 277 MPa) whereas 75A almost retains its room temperature strength up to 1300°C (from 320 to 312 MPa). The presence of glassy phase within 75A (see Fig. 9b) explains its relative decrease in flexural strength at high temperature. The glassy phase softens at 1300°C so that viscous flow phenomenon between mullite grains at the crack tip of a propagating crack would take place shielding the tip of the crack resulting in a decrease in the stress concentration [13, 14].

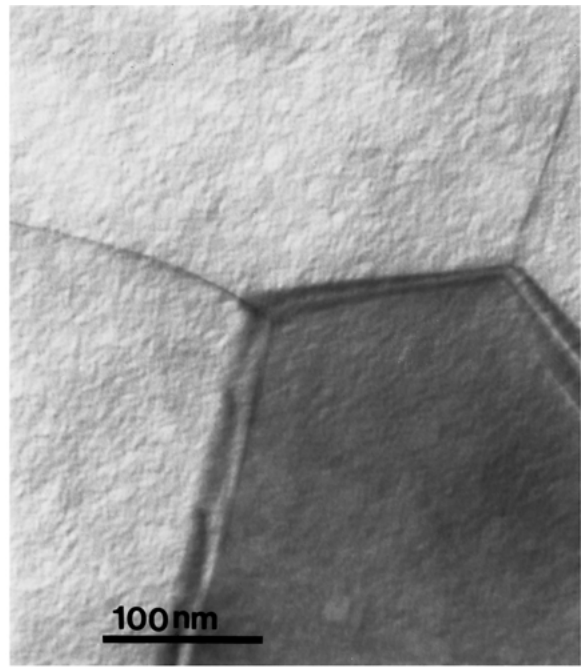


(a)

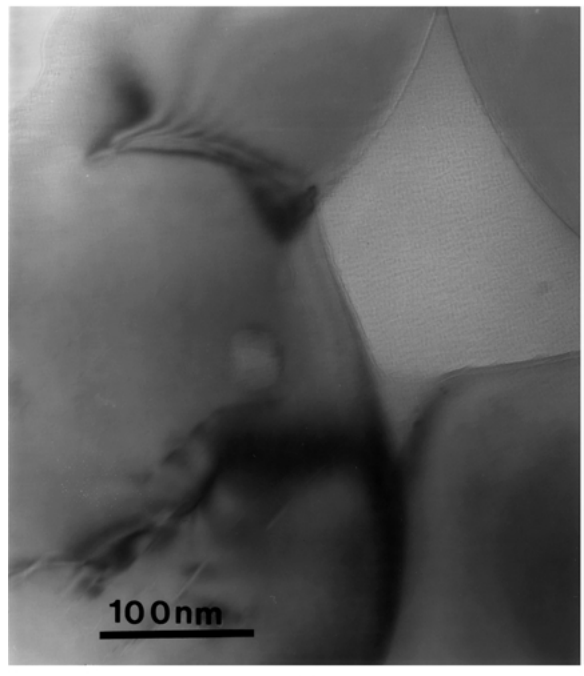


(b)

*Figure 9* TEM images of (a) 28M and (b) 75A mullites. Note the absence of any glassy phase within the mullite matrix produced from monophasic mullite sol (a).

By this way, crack propagation and catastrophic failure are prevented and the applied stress needs to be increased for the crack to propagate. The high resolution SEM images of fracture surfaces of 28M and 75A

TABLE III Room and high temperature 4-point flexural strength and fracture toughness of extruded 28M and 75A mullites

| | Flexural strength (MPa) | | Fracture toughness (MPa $m^{0.5}$) |
|---|---|---|---|
| | RT | 1300°C | RT |
| 28M | 345 ± 28 | 277 ± 46 | 2.8 ± 0.3 |
| 75A | 320 ± 33 | 312 ± 52 | 3.4 ± 0.4 |

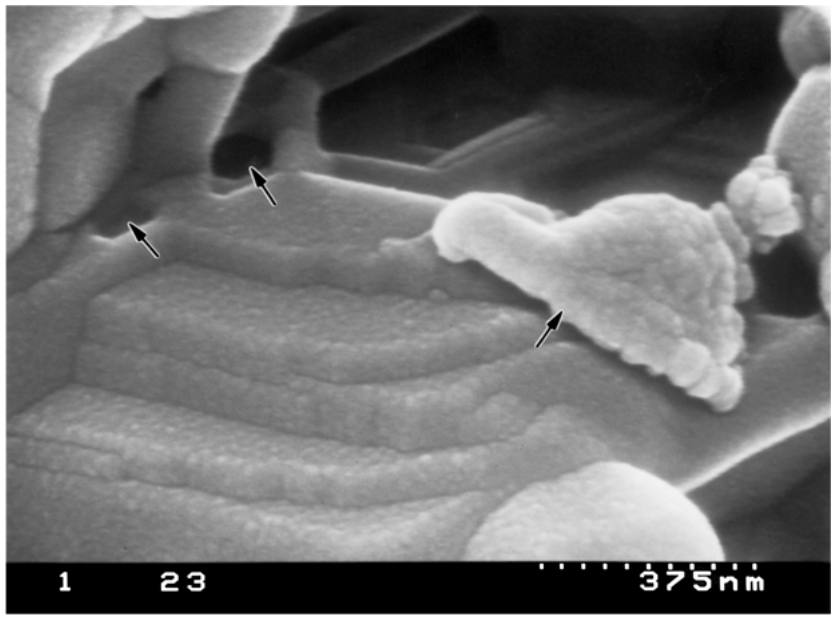


(a)

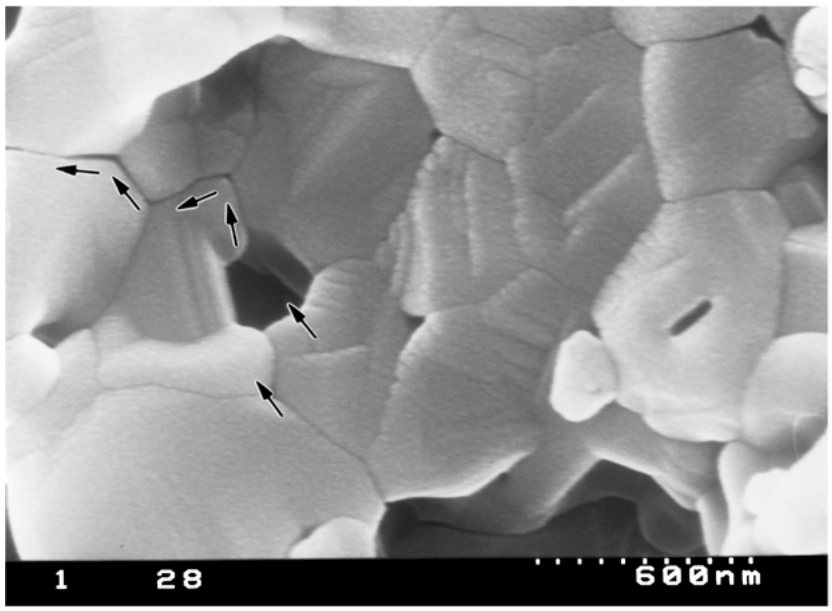


(b)

*Figure 10* Field emission gun SEM micrographs of fracture surfaces of (a) 28M and (b) 75A mullites after fracturing at 1300°C.

mullites after testing at 1300°C are shown in Fig. 10a and b, respectively. In this work, 5 wt% zirconia addition to mullite provided very small mullite grains within the sintered matrix which results in obtaining high flexural strength values at room temperature. Although the addition of small amount of zirconia to any monolithic ceramics is known as a grain growth inhibitor during sintering, it may also act as a natural flaw which initiates crack formation. As shown in Fig. 10, the fracture surfaces of 28M mullite after testing at 1300°C contain intragranularly failure of the mullite grains where a zirconia nano-agglomerate is located at the grain boundary therefore causing the initial crack to start growing from this point. The location of very fine pores (<200 nm) at the mullite grain boundaries was also visible from the micrograph shown in Fig. 10a, as pointed. Fig. 10b shows the fracture surface of 75A mullite subjected to flexural test at 1300°C indicating the presence of both inter- and intragranular fracture mode. Very fine pores (<300 nm) (located within the grains and also at the grain boundaries) and some zirconia agglomerates were also determined in 75A matrix as shown in Fig. 10b. In 75A, cracks initiate from a point where zirconia agglomerates and intergranular pore are present as pointed on the micrograph shown in Fig. 10b. It also shows that the crack initiates from the triple point propagates between the mullite grains which is the sign of glassy phase location along the grain boundaries that softens at this temperature thus results in slow crack growth until the final failure takes place.

Numerous research efforts on the development of mullite properties have led to the conclusion that the good mechanical and thermomechanical properties of mullite can be achieved if the three critical conditions are controlled [15–18]: (a) the presence of smaller pores (<1 $\mu$m), (b) uniform grain size and (c) no or less

glassy phase at the grain boundary. The relationships between flexural strength, fracture toughness, grain size and porosity of mullite ceramics were also reported and the following equations were derived [19]:

$$\sigma(\text{M Pa}) = ad^{-0.433}\exp(-0.036P) \quad (2)$$

$$K_{IC}(\text{M Pa m}^{0.5}) = bd^{0.182}\exp(-0.036P) \quad (3)$$

Where $a$ and $b$ are the constants, $d$ is the grain size and $P$ is the porosity (%). These equations clearly show that the flexural strength of mullite decreases and the fracture toughness increases with increasing grain size. Both mullite extrudates produced in this work showed similar sintered densities of 96.6 and 96.1% TD for 28M and 75A, respectively, therefore the main factors affecting the mechanical properties of the mullite are considered to be the grain/pore size, distribution and location and the presence of glassy phase within the matrix. The experimental findings in this work are in good agreement with the Equations 2 and 3 as shown in Table III. The higher fracture toughness value (3.2 M Pa $m^{0.5}$) of 75A is due to its coarser grain size (1.4 $\mu$m) compared to the toughness value (2.8 M Pa $m^{0.5}$) obtained from 28M that contains equiaxed mullite grains with an average grain size value of 0.94 $\mu$m. The average grain size of the two different mullites also explains the difference in their room temperature flexural strength. The higher the grain size the lower the flexural strength (345 and 320 M Pa for 28M and 75A, respectively). However, at high temperature from the TEM and SEM micrographs, it seems that the location of pores and glassy phase determine the mechanical performance of the mullites. As 28M mullite contains no glassy phase (see Fig. 9a), the inter- or intragranular failure of the matrix is governed by the presence of zirconia nano-agglomerates and nano-pores both located at the grain boundaries, as shown in Fig. 10a. In contrary, in 75A, nano-zirconia agglomerates and interganular pores initiate the cracks and the glassy phase along the grain boundary or at the triple grain junctions cause intergranular failure of the matrix, as shown in Fig. 10b. The relative decrease in strength at 1300°C could be attributed to the stress relaxation by softening of this glassy phase.

## 4. Conclusions

Stoichiometric 3:2 mullite extrudates with/without glassy phase were produced from monophasic (28M) and diphasic (75A) sol-derived mullite pastes using extrusion. No residual glassy phase was detected within the mullite matrix produced from 28M sol after pressureless sintering at 1400°C for 3 h. However, a glassy phase was observed at the triple junctions of mullite grains in a sample produced from 75A sol. Room temperature flexural strength and toughness of both mullites are determined by the grain size within the sintered mullite and 28M provides the highest strength (345 M Pa) as it contains equiaxed mullite grains with an average grain size of 0.94 $\mu$m. The presence and location of glassy phase and pores as well as nano-agglomerates along the grain boundaries seem to be determining the flexural strength of both mullites.


## Acknowledgement

This project (innovative processing of multiphase high temperature ceramics) was funded by the European Commission under the contract numbers BRITE-EURAM CT 97-0609. Project partners, namely, University of Warwick (UK), Morgan Materials Technology, $M^2T$ (UK), Centro de Estudios e Investigaciones, CEIT (Spain), Ecole des Mines de Paris (France) and Industria de Turbo Propulsores (Spain) are sincerely acknowledged for their contribution. Dr. Craig Freeman from $M^2T$ and Prof. P. Bowen from the Institute of Metallurgy and Materials (The University of Birmingham, UK) are acknowledged for providing the mullite raw materials and provision of high temperature test facilities, respectively.


## References


1. S. SOMIYA, R. F. DAVIS and J. A. PASK (eds.), "Ceramics Transactions" Vol. 6; Mullite and Mullite Matrix Composites. (American Ceramic Society, Westerville, OH, 1990).
2. S. KANZAKI, H. TABATA, T. KUMAZAWA and S. OHTA, *J. Amer. Ceram. Soc.* **68** (1985) C-6.
3. H. SCHNEIDER, H. OKADA and J. A. PASK (eds.), "Mullite and Mullite Ceramics" (John Wiley & Sons, Chichester, 1994).
4. B. E. YOLDAS, *J. Mater. Sci.* **27** (1992) 6667.
5. W.-C. WEI and J. W. HALLORAN, *J. Amer. Ceram. Soc.* **71** (1988) 581.
6. D. W. HOFFMAN, R. ROY and S. KOMARNENI, *ibid.* **67** (1984) 468.
7. C. KAYA, P. A. TRUSTY and C. B. PONTON, *Brit. Ceram. Trans.* **97** (1998) 48.
8. J. HULING and G. L. MESSING, *J. Non-Cryst. Solids.* **147/148** (1992) 213.
9. D. X. LI and W. THOMSON, *J. Amer. Ceram. Soc.* **73** (1990) 964.
10. Y. WANG and W. J. THOMSON, *J. Mater. Res.* **10** (1995) 912.
11. G. R. ANTIS, P. CHANTIKUL, B. R. LAWN and D. B. MARSHALL, *J. Amer. Ceram. Soc.* **64** (1985) 539.
12. M. I. MENDELSON, *ibid.* **52** (1969) 443.
13. C. KAYA, PhD thesis, The University of Birmingham, UK, June 1999.
14. C. KAYA, F. KAYA and A. R. BOCCACCINI, *Adv. Engineering Materials* **4** (2002) 21.
15. N. TAMARI, T. TANAKA, I. KONDOH and S. KOSE, *J. Ceram. Soc. Jpn.* **99** (1991) 89.
16. R. RUH, K. S. MAZDIYASNI and M. G. MENDIRATTA, *J. Amer. Ceram. Soc.* **71** (1986) 503.
17. K. RUNDGREN, P. ELFVING, H. TABATA and S. KANZAKI, *Ceram. Trans.* **6** (1990) 553.
18. C. NISCHIK, M. M. SEIBOLD, N. A. TRAVITZKY and N. CLAUSSEN, *J. Amer. Ceram. Soc.* **74** (1991) 2464.
19. Y. YAMADE, Y. KAWAGUCHI, N. TAKEDA and T. KISHI, *J. Ceram. Soc. Jpn.* D **14** (1990) 2.



*Received 27 February*
*and accepted 17 October 2002*